ACS APPLIED MATERIALS & INTERFACES

www.acsami.org

Forum Article

Heterogenized Pyridine-Substituted Cobalt(II) Phthalocyanine Yields Reduction of CO_2 by Tuning the Electron Affinity of the Co Center

Alberto De Riccardis, Michelle Lee, Roman V. Kazantsev, Alejandro J. Garza, Guosong Zeng, David M. Larson, Ezra L. Clark, Peter Lobaccaro, Paul W. W. Burroughs, Ermelinda Bloise, Joel W. Ager, Alexis T. Bell, Martin Head-Gordon, Giuseppe Mele,* and Francesca M. Toma*

Cite This: *ACS Appl. Mater. Interfaces* 2020, 12, 5251−5258

Read Online

ACCESS | Metrics & More | Article Recommendations | Supporting Information

ABSTRACT: Conversion of CO_2 to reduced products is a promising route to alleviate irreversible climate change. Here we report the synthesis of a Co-based phthalocyanine with pyridine moieties (CoPc-Pyr), which is supported on a carbon electrode and shows Faradaic efficiency ~90% for CO at 490 mV of overpotential (−0.6 V vs reversible hydrogen electrode (RHE)). In addition, its catalytic activity at −0.7 V versus RHE surpasses other Co-based molecular and metal−organic framework catalysts for CO_2 reduction at this bias. Density functional theory calculations show that pyridine moieties enhance CO_2 adsorption and electron affinity of the Co center by an inductive effect, thus lowering the overpotential necessary for CO_2 conversion. Our study shows that CoPc-Pyr reduces CO_2 at lower overpotential and with higher activity than noble metal electrodes, such as silver.

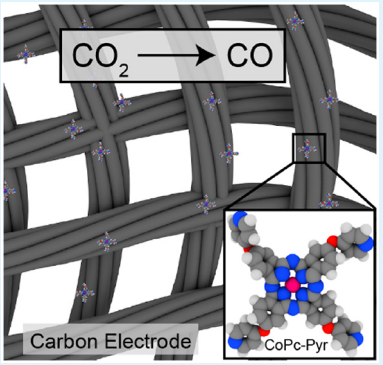

KEYWORDS: *phthalocyanine, CO_2 electroreduction, heterogenized catalysis, electronic properties, molecular catalyst*

1. INTRODUCTION

The need for renewable sources of sustainable energy has been a major scientific interest over the last several decades.[1,2] In this context, the conversion of carbon dioxide (CO_2) into chemical fuels is an attractive way to reach a sustainable energy future.[3,4] CO_2 removal from polluting sources could mitigate the effects of global warming,[5] while its conversion could provide a sustainable way to produce carbon-based fuels.[6−8] However, challenges such as the high stability of CO_2, its low reactivity to chemical transformation, and the lack of selectivity of many existing catalysts toward narrow product distributions hamper progress in this field. Researchers have tried to address this problem by electrochemical CO_2 reduction (CO_2R) using various metallic electrodes as electrocatalysts.[9,10] The advantage of electrochemistry mainly lies in its compatibility with renewable energy sources such as solar photovoltaics, while allowing the possibility to alter the reaction pathway by tuning the applied potential. However, there are also several drawbacks. When electrochemical CO_2R is performed in an aqueous environment, it is always in competition with the undesired hydrogen evolution reaction (HER).[11] As such, an ideal CO_2R catalyst should selectively guide CO_2 to the desired product while minimizing parasitic current to H_2 production. Successful CO_2R has been demonstrated using transition-metal catalysts,[12] semiconductors,[13,14] and metal ion complexes.[15] However, while these catalysts exhibit activity for CO_2R, problems with stability and poor selectivity limit their commercial applicability.

Among all of the CO_2R products, carbon monoxide (CO) requires the lowest overpotential to obtain, and its industrial importance as a feedstock for Fischer−Tropsch chemistry makes it an attractive target. While CO can be produced electrochemically on silver or gold, there is a need for a more abundant electrode material to facilitate this conversion. In this view, molecular catalysts based on cyclam, porphyrin, and phthalocyanines offer the possibility to have high selectivity and high yield for CO_2R by using non-noble metals.[15] In particular, phthalocyanines are a class of aromatic molecules with good chemical and thermal stability that are known to be efficient catalysts for a wide range of reactions that make them a promising choice for CO_2R electrocatalysis, including generating product mixtures of CO and H_2 under CO_2R conditions.[16−20] Co(II)- and Fe(II)-based examples were found to be effective in (photo)electrocatalytic CO_2 reduction producing CO and formate.[21,22] Nonetheless, while the catalytic properties of Co(II) phthalocyanine (CoPc) have

Special Issue: Young Investigator Forum

Received: October 19, 2019
Accepted: January 6, 2020
Published: January 23, 2020

been known for several decades, there are limited examples of highly selective CO_2R at lower overpotentials.[23,24] Continued research in catalyst modification could bring about the desired properties in phthalocyanine catalysts.

Apart from tuning the electronic properties of the molecular catalysts with coordinating molecules in the axial position,[25] building composite electrodes is equally important to integrating molecular catalysts into electrodes.[15,26] For example, Kramer et al. showed that grafting CoPc onto a pyridine-substituted polymer increases the selectivity of CO likely due to axial coordination with the metal center.[27,28] In its application with phthalocyanine, pyridine has been used as a ligand for the metal center, limiting its use as coordinating agent.[29] Pyridine's other possible role as a peripheral substituent could yield changes to the catalytic properties by either changing the electronic density on the macrocycle or giving another catalytic path versus the one that involves coordination of CO_2 to the Co(II) center.[24,30]

Herein, we report the synthesis of a pyridine-substituted cobalt phthalocyanine (CoPc-Pyr) and compare its activity with a non-substituted one (CoPc). We fabricate a composite electrode by supporting these derivatives onto a carbon paper. The heterogenized compound shows the beneficial effect of the pyridine moieties on the selectivity for CO and on the onset potential for CO_2 reduction measuring a Faradaic efficiency (FE%) ~90% for CO at only 490 mV of overpotential (−0.6 V vs reversible hydrogen electrode (RHE)). To the best of our knowledge, this may be the highest FE for CO at this overpotential and is higher than the one obtained for CO with CoPc in the same identical conditions. This finding is supported by our density functional theory (DFT) calculations, which show that the pyridine substituents provide an inductive effect to enhance CO_2 adsorption and the electron affinities of the metal center, resulting in lower overpotentials and greater selectivity for CO_2R versus HER.

2. EXPERIMENTAL SECTION

2.1. Methods and Instruments. FT-IR spectra were recorded on a JASCO FT-IR 660 Plus spectrometer. NMR spectra were recorded on a Bruker Avance 400 (400 MHz) using $CDCl_3$ as solvent. Product detection data were acquired by Agilent Mass Hunter system software (version 6.0). The mass spectrometer was operated in full-scan mode in the m/z range of 100−1000.

The surface chemical composition was obtained by X-ray photoelectron spectroscopy (XPS) on a Kratos Axis Ultra DLD system at a takeoff angle of 0° relative to the surface normal at room temperature. An aliquot of 100 μL of 1×10^{-4} M CoPc-Pyr in trifluoroethanol (TFE) was dropcasted onto silicon wafer. It was air-dried for 18 h. A monochromatic Al Kα source ($h\nu$ = 1486.6 eV) was used to excite the core-level electrons of the material. C 1s, N 1s, O 1s, and Co 2p core levels were collected, with pass energy of 20 eV, step size of 0.05 eV, and eight sweeps each to obtain a good signal-to-noise ratio. The sample was loaded to the chamber a day prior to the measurement to achieve a good vacuum condition (7.5×10^{-9} Torr). Spectral fitting was conducted using CasaXPS analysis software. Spectral positions were corrected using adventitious carbon by shifting the C 1s core level position to 284.8 eV.

UV−Vis spectra in solution were obtained on a Shimadzu SolidSpec-3700 UV/vis/NIR spectrometer (NIR = near-infrared). A diluted solution of Co-Pc-Pyr (**4**) was prepared in TFE, dimethylformamide (DMF), or ethyl acetate. In addition, two CoPc-Pyr (**4**) modified electrodes were placed into a centrifuge tube after electrochemical testing. An aliquot (5 mL) of TFE was added to dissolve ~4.6×10^{-9} mmol of CoPc-Pyr, which underwent electrochemical CO_2 reduction. It was vortexed for 30 s to ensure that almost all of the CoPc-Pyr on the electrodes dissolved in TFE. This solution was used for UV−vis analysis.

Inductively coupled plasma mass spectrometry (ICP-MS) measurements were performed with an Agilent 7900 using a standard configuration consisting of Micromist nebulizer and quartz sample introduction system of Scott type with a spray chamber and a one-piece torch with a 2.5 mm inner diameter injector; Ni cones were used throughout. Internal standards were added online via the sample delivery peristaltic pump. The instrument was optimized using default autotune conditions directly from the MassHunter Workstation for U-HMI. Samples were measured in helium collision mode for all analytes.

Electrochemical measurements were performed in an electrochemical cell made from poly(ether ether ketone) (PEEK) in-house using a commercial benchtop milling machine from Othermill. Each half-cell is 5.1 cm wide, 5.1 cm tall, and 1.27 cm thick. Each half has a circular hole on one face with a radius of 0.64 cm, which slopes to an opening on the other face that is two semicircles separated by 0.64 cm to form an oblong circle. The electrochemical cell was cleaned in 20% nitric acid in Millipore water overnight. Then, the cell was rinsed with Millipore water three times and sonicated in Millipore water for 30 min. It was dried with nitrogen gas before it was assembled for electrochemically testing the fabricated working electrodes. On the cathode side three ports were added, one on the bottom for the CO_2 inlet (through a glass frit of Adam & Chittenden), one on the side for Ag/AgCl reference electrode (LF-1, 1.0 mm outer diameter, Innovative Instruments, Inc.), and a third one on the top for gas chromatography (GC) connection. On the anode side, only one port for O_2 evolution was added. The two electrodes (working and counter) were placed and sealed against the external part of the compartment through two squeezing plates of polyethylene. Seals between layers were created with Viton o-rings inserted into milled channels in the PEEK half cells, and a Selemion membrane was placed between the two compartments. The gas flow was maintained by Alicat mass flow controllers with mass flow meters downstream to leak check. Product detection analysis was conducted in such homemade electrochemical cell by using Pt as counter electrode and 0.05 M K_2CO_3 (99.995%) as electrolyte.[31] The two compartments of the cell were divided by a Selemion membrane, and CO_2 was continuously purged in the cell during all of the experiment at a flow rate of 5 sccm. The gaseous products were detected by in-line Shimadzu 490GC, while the liquid products were analyzed using UltiMate 3000 HPLC at the end of the electrochemical experiment.

The procedure for taking into account the impedance compensation in the calculation of the applied voltage was similar to the one reported by Kuhl et al.[12] Briefly, impedance spectroscopy was performed to calculate the resistance of the solution that normally is not compensated by the potentiostat, and that causes a voltage drop between the reference and the working electrode. A measurement of the real and imaginary contribution to the impedance at open-circuit voltage at various frequencies was performed. Considering that, at high frequency, the contributions to the impedance other than the resistance of the solution are negligible, a scan from 100 Hz to 0.5 MHz was performed. 5 kHz was found to be the appropriate frequency to determine only the real contribution to the resistance solution, and this value was used for all of the measurements. The potentiostat was allowed to compensate for the resistance at 5 kHz for the 85% (after this value the current becomes instable) of its total value; the remaining 15% was manually compensated after the measurement using Ohm's law $V = IR$.

Cyclic voltammograms (CVs) were collected after 20 min of CO_2 purging at 5 sccm to register the performance of the electrode. The chronoamperometry measurement (CA) started while continuously flowing the gas. A constant potential was applied for 40 min, and after 10 min samples were taken every 10 min. Each CA was repeated three times with three different electrodes, and the results reported are the average of the three measurements. Another CV was registered at the end of each experiment to look for any eventual modification of the electrode after the CA. Both H_2 and CO were detected on two

https://dx.doi.org/10.1021/acsami.9b18924
ACS Appl. Mater. Interfaces 2020, 12, 5251−5258

different molecular sieve columns (MOL 5A-Agilent): for H_2 detection, helium was used as balance gas, and the temperature of the column was maintained constant at 170 °C as well as the pressure (207 kPa); for CO detection, N_2 was used as balance gas.

Turnover frequency (TOF) calculations are based on Faradaic efficiency (FE) and current using

$$\mathrm{TOF} = \frac{\mathrm{Q} \times \mathrm{FE}}{t \times N \times F \times n_{\mathrm{catalyst}}} = \frac{i \times \mathrm{FE}}{N \times F \times n_{\mathrm{catalyst}}}$$

where Q is the total charge passed in time t, i is the current, FE is the Faradaic efficiency for the desired product, N is the number of electrons in the half reaction ($N = 2$ for CO_2 to CO conversion), F is the Faraday constant ($F = 964\,85$ C/mol electrons), and n_{catalyst} is the mole of catalyst CoPc-Pyr deposited onto the active area of carbon paper. n_{catalyst} was quantified by coulometric methods by integrating the current of the cyclic voltammograms at ∼0.25 V versus RHE and ∼0.1 V versus RHE peaks for CoPc-Pyr and CoPc, which corresponds to the Co(II) → Co(I) reduction. The loading for CoPc-Pyr was estimated to be 10^{-8} moles, whereas the loading for the CoPc was estimated to be 2.3×10^{-9} moles. The total amount of CoPc-Pyr and CoPc loaded onto the electrode was measured by ICP-MS and estimated to be on the order of 10^{-8} moles in both cases. TOF calculations were based on the number of active catalysts measured electrochemically.

Spin-unrestricted DFT calculations were performed using the Gaussian suite of programs. Geometries were optimized at the ωB97X-D/6-31G(d,p) level, and the reported energies were computed with the same method but adding diffuse functions to heavy atoms (i.e., 6-31+G(d,p) basis), to better describe negatively charged ions (test calculations indicate that the addition of diffuse functions can affect energies and Mulliken charges significantly but not the geometries, which are rather constrained due to conjugation). All calculations used the polarizable continuum model (PCM) to model solvent effects (water). The IQmol software was used for orbital visualization and analysis of results. Energies for reactions involving simultaneous proton and electron transfer were computed using the computational hydrogen electrode model. Zero-point energy (ZPE) and vibrational thermal corrections were calculated according to the rigid-rotor/harmonic-oscillator interpolation method of Grimme.[32]

2.2. Materials. DMF, potassium carbonate, dichloromethane, methanol, hydrochloric acid, 1,8-diazabicyclo[5.4.0]undec-7-ene (DBU), 1-hexanol, dimethyl sulfoxide (DMSO), 4-nitrophthalonitrile, and 4-hydroxy-pyridine were purchased from Sigma-Aldrich. And, they were used as received. Selemion AMV anion-exchange membrane was purchased from AGC Engineering Co., Ltd. Carbon paper (Sigracet 29BC) was purchased from Fuel Cell Store. Carbon dioxide (99.995%) and nitrogen (99.999%) were obtained from Praxair.

*2.2.1. Synthesis of 4-(4-Oxypyridinyl)phthalonitrile (**3**).* 4-(4-Oxypyridinyl)phthalonitrile (**3**) was synthesized with the following procedure (Scheme S1, Supporting Information): in a 50 mL round-bottom flask, 4-nitrophthalonitrile (**2**) (5.78 mmol, 1.0 g) was mixed with 4-hydroxypyridine (**1**) (6.31 mmol, 600 mg). Thirty milliliters of DMSO were added. The solution was heated at 60 °C, and K_2CO_3 (14.5 mmol, 2.0 g) was slowly added. The suspension was then heated at reflux for 16 h under N_2 atmosphere. The crude of reaction was filtered to remove all the unreacted K_2CO_3, and 100 mL of water were added to the filtrate. A solution of CH_2Cl_2/methanol (MeOH) 5% was used to extract the product of synthesis from the water/DMF solution. The complete extraction was followed by thin-layer chromatography (TLC) (R_f of PyO_Pn ≈ 0.46 in CH_2Cl_2/MeOH 10% solution). The organic solvent was removed under low pressure. The pale yellow solid was dried in an oven at 60 °C. A second step of purification was needed to remove the unreacted **1** from the obtained powder. The powder was washed several times with a small volume of 10% NaOH solution. Various isomers of **3** (700 mg, 55% yield) were obtained. The final product was characterized with ^{1}H NMR (Figure S1, Supporting Information), ^{13}C NMR (Figure S2, Supporting Information), and Fourier transform infrared (FTIR) spectroscopy (Figure S3, Supporting Information).

*2.2.2. Synthesis of CoPc-Pyr (**4**).* CoPc-Pyr (**4**) was synthesized in the following way (Scheme S2, Supporting Information): the isomers mixture of **3** (2.71 mmol, 600 mg) was added into a 50 mL three-necked round-bottom flask. Excess of cobalt acetate ($Co(OAc)_2$) (0.50 mmol, 125 mg) was added into the flask. They were dissolved in 5 mL of 1-hexanol. The reaction was heated under inert atmosphere (N_2). Once the reflux temperature (160 °C) was reached, DBU (0.20 mmol, 30 μL) was added to the reaction. The color of solution turned from pale yellow to light blue, the intensity of which intensified during the time. The reaction refluxed for 12 h. The solvent was removed under low pressure. The blue precipitate was washed several times with HCl solution (pH = 3) and with MeOH to eliminate the unreacted precursor. **4** is soluble in DMF, DMSO, and partially in trifluoroethanol and 1 M HCl solution. The final product was characterized with FTIR (Figure S4, Supporting Information), XPS (Figures S5−S8, Supporting Information), and UV−vis (Figure S9, Supporting Information).

2.3. Electrode Preparation. The carbon paper electrode (Sigracet 29BC) was cut in a circle with a diameter of 1.25 cm and immersed for 15 min in 65% HNO_3 to remove iron impurities possibly present in the fibers. Application of the catalyst to the electrode was achieved by dip coating. The carbon paper was dip-coated for 1 min in a solution of 10^{-4} M CoPc-Pyr in trifluoroethanol and 10^{-4} M CoPc-Pyr in DMF solution and allowed to dry overnight under vacuum at 80 °C to remove the possible trace of solvent. The same procedure was followed also for the CoPc catalyst. In particular, 23.2 mg of CoPc was dissolved in 4 mL of DMF resulting in a 0.6×10^{-3} M solution of phthalocyanine in DMF. This solution was further diluted to obtain the dip-coating solution. The final loading of catalyst on the carbon electrode was estimated to be $\sim 2.3 \times 10^{-9}$ mmol by integration of the cyclic voltammetry peak at ∼0.14 V versus RHE.

3. RESULTS AND DISCUSSION

The CoPc-Pyr was synthesized by cyclotetramerization of its precursor in the presence of Co(II) salt. Briefly, a nucleophilic substitution of a nitro group on 4-nitrophthalonitrile by 4-hydroxypyridine gave the phthalocyanine precursor, which was cyclotetramerized in the presence of cobalt acetate (see Experimental Section, Scheme 1, and Figures S1−S9 in the Supporting Information for full details). To assess the catalytic performance of CoPc-Pyr, cyclic voltammetry of both CoPc and CoPc-Pyr heterogenized on a carbon paper electrode was performed under CO_2 and N_2 atmosphere to determine catalytic activity (Figure 1).

Scheme 1. Synthesis of Phthalocyanine-Based CO_2 Reduction Catalyst

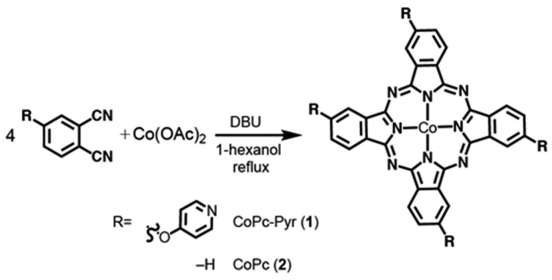

The electrochemical reduction of CoPc in the absence of CO_2 shows a reversible peak around 0.15 V versus RHE and a quasi-reversible one at −0.4 V versus Ag/AgCl. The first redox couple arises from the reduction of Co(II) to Co(I) (generating $[Co(I)Pc\text{-}Pyr]^{1-}$), while the second reduction produces $[Co(I)Pc\text{-}Pyr^{\cdot-}]^{2-}$, where the charge can be

https://dx.doi.org/10.1021/acsami.9b18924
ACS Appl. Mater. Interfaces 2020, 12, 5251−5258

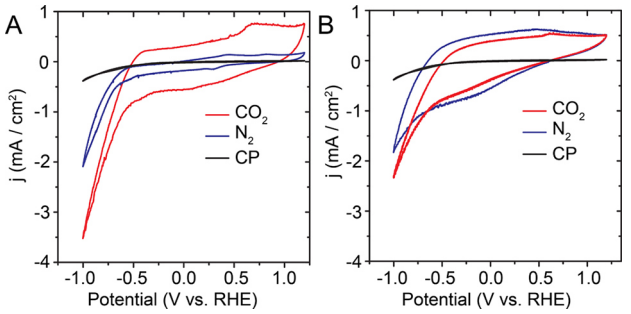

Figure 1. Cyclic voltammetry of CoPc-Pyr (A) and CoPc (B) deposited on carbon paper under CO_2 (red) and N_2 (blue) atmospheres in 0.05 M K_2CO_3 at 100 mV/s with 5 sccm for the flow rate of CO_2 (pH = 6.8). CV of carbon paper (Cp) in CO_2 atmosphere (black) is reported for comparison.

delocalized onto the macrocycle. These peaks are still present, even if slightly shifted, when the solution is saturated with CO_2. Moreover, the second peak is closely associated with the potential for CO_2 reduction (−0.4 V vs RHE), suggesting that $[Co(I)Pc\text{-}Pyr\cdot^{-}]^{2-}$ is the catalytically active species.

To assess the CO_2R abilities of CoPc-Pyr and the resulting product distribution, we loaded the CoPc-Pyr on a carbon paper electrode and used it as a cathode in a custom reaction cell consisting of a Pt counter-electrode and Selemion membrane (Figure 2a,b; see Experimental Section for additional details).

For CoPc-Pyr, a high FE% for CO (95%) can be measured at low potential (−0.7 V vs RHE at pH 6.8). Interestingly, good selectivity (2:1 CO/H_2) for the CO_2R is still present at very low current and more positive potential (−0.45 V vs RHE). Considering that the thermodynamic potential for CO formation is −0.11 V versus RHE and that this potential is increased by the reaction kinetics, the CoPc-Pyr shows a

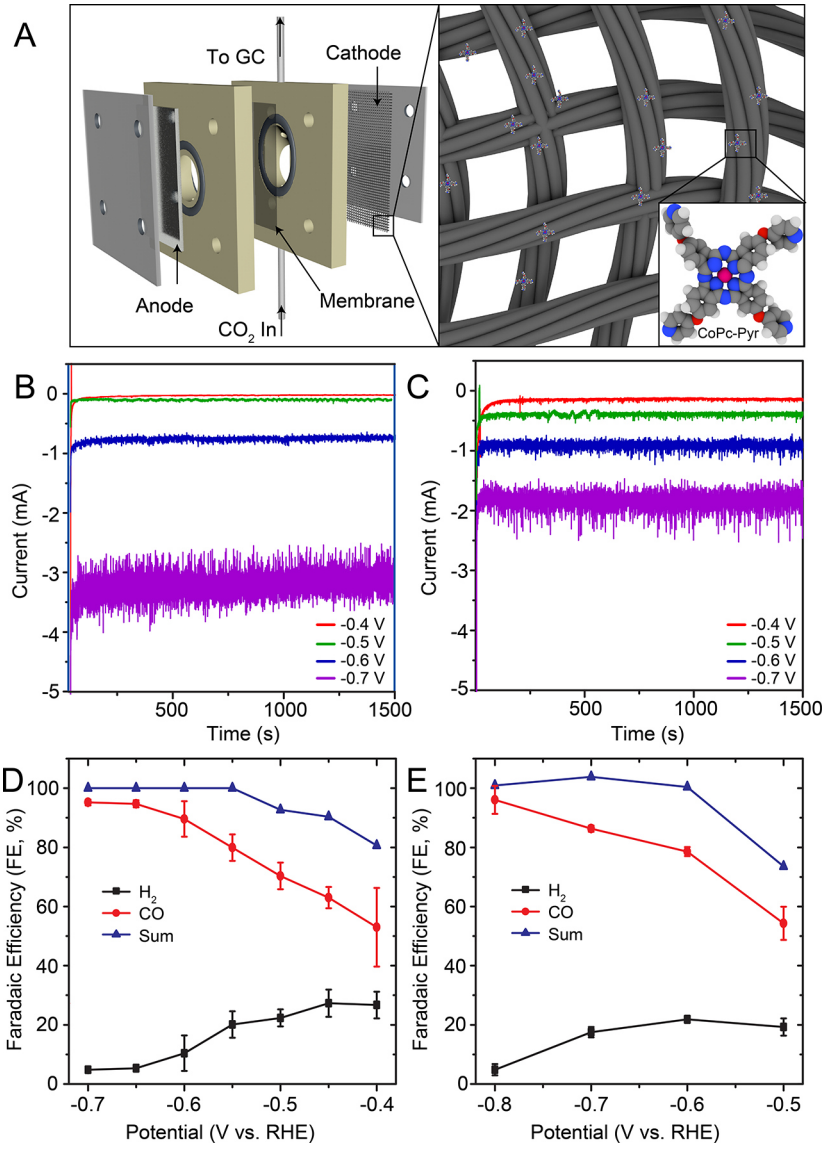

Figure 2. (A) Schematic of a two-chamber electrochemical cell used for CO_2R experiments (left). Carbon paper cathode with physisorbed CoPc-Pyr used as working electrode (right). Chronoamparometry measurements for (B) CoPc-Pyr and (C) CoPc at various potentials under CO_2R conditions vs RHE. Faradaic efficiency plots for (D) CoPc-Pyr and (E) CoPc. For the sake of completeness, a full list of the chronoamperograms at all different potentials tested for CoPc-Pyr are reported in the Supporting Information (Figure S10).

https://dx.doi.org/10.1021/acsami.9b18924
ACS Appl. Mater. Interfaces 2020, 12, 5251−5258

Table 1. Activity Comparison of Highly Efficient Co-Based Electrocalysts[a]

catalyst	applied potential (V vs RHE)	electrolyte	FE CO	current density (mA/cm^2)	TOF (s^{-1})	ref
CoPc-Pyr	−0.7	0.05M K_2CO_3	95%	2.5[b]	6.9	this study
CoPc	−0.7	0.05M K_2CO3	86%	1.3[b]	3.5	this study
perfluorinated CoPc	−0.8	0.5 M $NaHCO_3$	93%	4.4	1.6	19
CoPc-P4VP	−0.7	0.1 M NaH_2PO_4	92%	2.9	6.3	28
COF-367-Co	−0.7	0.5 M $KHCO_3$	91%	3.3	0.04	34
COF-367-Co (10%)	−0.7	0.5 M $KHCO_3$	70%	1.4	0.1	34
COF-367-Co (1%)	−0.7	0.5 M $KHCO_3$	40%	0.45	0.2	34

[a]These testing conditions were chosen for each catalyst to lead to best performance, and more details are reported in the original citations. [b]Current density was obtained by dividing the measured current by the area of the electrode (1.25 cm^2, see Experimental Section).

reduced overpotential of 290 mV for conversion of CO_2 to CO. CoPc-Pyr is also able to catalyze the conversion of CO_2 to CO with a FE% ∼90% at −0.6 V versus RHE (490 mV of overpotential). In contrast, CoPc has an overpotential of 390 mV for conversion of CO_2 to CO and catalyzes the conversion of CO_2 to CO with ∼80% FE at −0.6 V versus RHE. Compared to polycrystalline Ag, which is one of the most selective catalysts for CO_2 to CO formation and which shows an onset potential for CO_2 reduction ca. −0.7 V versus RHE and 98% FE for CO at −1.0 V versus RHE,[33] CoPc-Pyr has an onset for the CO_2R more positive than noble-metal electrode.

In addition to its high selectivity toward CO production, CoPc-Pyr demonstrates high catalytic performance for CO_2 reduction to CO. Considering the electrochemically active CoPc-Pyr (10^{-8} moles), at applied potential of −0.7 V versus RHE, the catalyst has turnover frequency of 6.9 s^{-1} while maintaining its selectivity at 95% FE to CO (Table 1, Table S1). The Pyr moiety increases the FE for CO and doubles the TOF with respect to the unsubstituted derivative at −0.7 V versus RHE. The CoPc-Pyr catalyst has similar selectivity but higher TOF when compared to perfluorinated CoPc, when the latter operates at a slightly higher overpotential (−0.8 V vs RHE). Compared to CoPc-P4VP, the electrode where CoPc immobilized in a poly(4-vinylpyridine) (P4VP), CoPc-Pyr has slightly higher TOF and more pronounced CO selectivity.[28] Compared to other heterogeneous cobalt catalysts with 4-N ligand like COF-367-Co, CoPc-Pyr shows significantly higher catalytic activity and selectivity.[34] It is noted that, as reported by Liang, Wang and co-workers, immobilization of the catalyst on carbon nanotubes may help to further decrease the measured overpotential.[35] In addition, Manthiram and co-workers suggest that, due to aggregation of catalysts with extended $\pi-\pi$ networks, optimization of the catalyst loading on the electrode could have a positive effect on increasing the apparent TOF of the catalyst.[23] In this view, CoPc-Pyr has a more extended $\pi-\pi$ network than CoPc that can aid aggregation, whereas its structure causes increased steric hindrance and, hence, inhibits aggregation. This observation is also supported by DFT calculations (vide infra), where it is shown that the core of the Pc and the pyridine rings are not coplanar.

Chronoamperometric measurements show a stable current during operation for both catalysts, thus supporting no degradation of the molecules or decrease in activity (Figure 2B,C). In addition, UV−vis spectroscopy of the CoPc-Pyr catalyst recovered from the carbon paper electrode after performing CO_2R measurements supports no degradation of the molecular catalyst during CO_2R (Figure S11). A few studies have shown the stability of similar complexes, and they have concluded that CO does not originate from catalyst degradation.[23,24] At −0.7 V versus RHE, CoPc-Pyr has a higher current than CoPc, while maintaining higher selectivity as already mentioned. Moreover after 5 h of electrolysis at various potentials, CoPc-Pyr is still able to catalyze the CO_2 to CO conversion without significant difference in the measured current. Both of the molecules are not soluble in water at pH 6.8, so homogeneous catalysis can be excluded as well. We analyzed the FE for H_2 and CO, when CoPc-Pyr or CoPc are used as catalysts in a CO_2 atmosphere as a function of potential (Figure 2D,E). CoPc-Pyr has a higher selectivity for CO with respect to CoPc at same potential (Table 1, Table S2). The only product other than CO detected is H_2, and the sum of the FE accounts for all of the current.

Interestingly, while CoPc and tetraphenylporphyrin modified with electron-withdrawing ligands show improved CO_2R activity, a complete mechanistic interpretation is still missing.[20] To understand how the presence of the pyridine moiety tunes the selectivity for CO generation, we calculated the binding energy of the different intermediates that yield CO or H_2. Specifically, the formation of CO proceeds through a *COOH intermediate that further extracts a proton from water and yields CO through liberation of a water molecule.[36] Thus, as an indicator of the selectivity between the CO_2R and formation of H_2, we considered the relative energy for binding an intermediate that leads to the CO, E^*_{COOH}, compared to the binding energy for an intermediate that leads to H_2 (the catalyst bound to a proton), E^*_H. In agreement with experiment, the DFT calculations predict higher selectivity of both molecules for CO_2R with respect to H_2 production, with $E^*_{COOH} < E^*_H$. In addition, the computed binding energies for CoPc and CoPc-Pyr are very similar, although the values of E^*_{COOH} and E^*_H are consistently lower for CoPc-Pyr. This finding is a consequence of the higher electron affinity of CoPc-Pyr as compared to CoPc (see Table 2 and discussion below), as the binding of H and COOH both involve reduction steps.

Our DFT calculations also support the experimental finding that CoPc-Pyr is the superior catalyst. Table 2 summarizes the computed energies of various reactions (for both CoPc and CoPc-Pyr) that are related to properties such as CO_2 and electron affinities (EAs). According to these results, the binding of CO_2 to the monoanion is very weak (0.05 eV). This binding energy is insufficient to overcome the entropy of CO_2 in solution (0.18 eV)[37] at room temperature; thus, the driving force for CO_2 to bind to the monoanion species is minimal (ΔG_{bind} = +0.13 eV; enthalpic contributions are negligible). In contrast, CO_2 attaches to the dianion with a binding energy of 0.33 eV. This energy is large enough to overcome the loss in entropy due to binding and favor

https://dx.doi.org/10.1021/acsami.9b18924
ACS Appl. Mater. Interfaces 2020, 12, 5251−5258

Table 2. Calculated Energies[a]

reaction	CoPc	CoPc-Pyr
$CoPc + e^- \rightarrow [CoPc]^-$	−4.36	−4.50
	−4.38	−4.62
$[CoPc]^- + e^- \rightarrow [CoPc]^{-2}$	−2.97	−3.10
	−3.08	−3.18
$[CoPc]^- + CO_2 \rightarrow [CO_2\text{-}CoPc]^-$	−0.11	−0.05
	−0.06	0.02
$[CoPc]^{-2} + CO_2 \rightarrow [CO_2\text{-}CoPc]^{-2}$	−0.37	−0.33
	−0.21	−0.22
$[CoPc]^- + H^+ + e^- \rightarrow [H\text{-}CoPc]^-$	0.39	0.36
	0.55	0.53
$[CoPc]^- + CO_2 + H^+ + e^- \rightarrow [HOOC\text{-}CoPc]^-$	0.03	−0.01
	0.45	0.42

[a]Calculated energies (in eV) of reduction and CO_2 adsorption to CoPc and CoPc-Pyr. The second energy value in each reaction includes the zero-point energy and vibrational thermal corrections according to the rigid-rotor/harmonic-oscillator interpolation method of Grimme.[32]

formation of the $[CO_2{-}Co(I)Pc\text{-}Pyr]^{-2}$ adduct (ΔG_{bind} = −0.14 eV).

The lower onset potential for CO_2 reduction of CoPc-Pyr as compared to CoPc can be rationalized by two observations that have been already pointed out: (1) that the catalytically active species is the dianion ($[Co(I)Pc]^{-2}$ or $[Co(I)Pc\text{-}Pyr]^{-2}$) and (2) that CoPc-Pyr has a higher electron affinity than CoPc (and thus is easier to reduce). Indeed, the computed electron affinities (Table 2) of $[Co(I)Pc\text{-}Pyr]^{-1}$ and $[CO_2{-}Co(I)Pc\text{-}Pyr]^{-1}$ are, respectively, 0.24 and 0.14 eV higher than for their unsubstituted counterparts, which correlates well with the 0.15 eV difference between the CO_2R onset potential of the two catalysts. The DFT-optimized structure of CoPc-Pyr shown in Figure 3 suggests that steric interactions break the conjugation

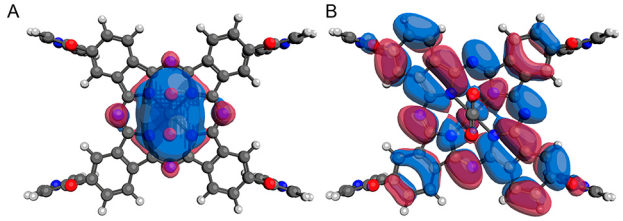

Figure 3. HOMO-2 (A) and HOMO (B) for the DFT-optimized structure of $[CO_2{-}CoPc\text{-}Pyr]^{-2}$. The spin state is a doublet, and the geometry of CO_2 is bent. The HOMO-2 is the main orbital responsible for the catalyst−CO_2 interaction, involving the d_{z^2} orbtials of the metal and the π^* orbitals of CO_2.

between the pyridine groups and the core of the catalyst, because the phthalocyanine and pyridine rings are not coplanar. In turn, this characteristic indicates that the greater electron affinity of the CoPc-Pyr is due to electron-withdrawing inductive effects of the oxygen atoms linking the pyridine rings to the phthalocyanine. Combining these observations with the experimental results reported here implies that one may enhance the selectivity and lower the onset potential for the CO_2R of a CoPc catalyst by subtle changes on the electron affinity of the catalyst via substituents that act, effectively, as electron-withdrawing groups. A more drastic increase in electron affinity may not be as effective due to the possibility of reducing the affinity for electrophilic CO_2 too much, hindering the necessary first step of CO_2 binding.

In addition to the optimized structure of $[CO_2{-}CoPc\text{-}Pyr]^{-2}$, Figure 3 shows the isosurfaces for two molecular orbitals that reveal properties of the catalytic species. The first orbital shown, the HOMO-2 (HOMO = highest occupied molecular orbital), is the main orbital responsible for the CO_2−catalyst interaction. The metal's d_{z^2} orbitals donate electron density to the π^* orbitals of CO_2 in a bonding interaction. Thus, the cobalt center is acting as a Co(I) in a tetrahedral crystal field, which makes the filled d_{z^2} orbital the highest occupied energy level localized on the metal. Although it seems unintuitive to have the HOMO-2 as being responsible for the bonding between CO_2 and the catalyst, other researchers have made analogous observations for cobalt porphyrins.[38] The second orbital shown is the HOMO, which is singly occupied for the doublet spin state that was calculated. The shape of this orbital suggests delocalization over the phthalocyanine ring of this single electron, in agreement with what has been deduced from experiments. It is also worth mentioning that the structure of CO_2 is bent when attached to the complex and that the sum of its Mulliken charges is −0.64, corroborating the formation of a negatively charged CO_2 when it binds to the catalyst.

CONCLUSION

In conclusion, we have shown the synthesis of a Co-based phthalocyanine bearing pyridine groups, which has been heterogenized on a carbon paper support and tested for CO_2R. We have demonstrated that the pyridine groups are responsible for reducing the overpotential for conversion of CO_2 to CO with respect to unfunctionalized phthalocyanine. DFT calculations support the idea that the overpotential reduction is due to an enhanced energy of CO_2 adsorption and greater electron affinity of the Co center induced by the pyridine moieties. On the one hand, through a combination of experimental evidence and DFT calculations, we show that the presence of electron-withdrawing groups may beneficially tune the electron affinity of the catalyst, thereby increasing the activity of a CoPc derivative for CO_2R. On the other hand, a drastic increase in electron affinity can also inhibit CO_2 binding thus hindering CO_2R. Striking a fine balance between these two effects can aid the design of novel, efficient molecular catalysts for CO_2R. In addition, this study shows that heterogenized molecular catalysts exhibit improved overpotential and selectivity to CO_2R versus HER than noble-metal catalysts, thus providing a tunable route to CO production with good energy efficiency using more earth-abundant elements.

ASSOCIATED CONTENT

Supporting Information

The Supporting Information is available free of charge at https://pubs.acs.org/doi/10.1021/acsami.9b18924.

Reaction schemes, FTIR, NMR, XPS, and UV−vis data of the synthesized compounds. Additional chronoamperometry data for CoPc-Pyr (**4**) and Vis spectrum of the material recovered from the electrode after the electrochemical CO_2 reduction compared to the starting CoPc-Pyr (**4**). Table used for calculation of turnover frequency values (PDF)

All the source data that support the findings of Figures 1a,b and 2b−e (XLSX)

https://dx.doi.org/10.1021/acsami.9b18924
ACS Appl. Mater. Interfaces 2020, 12, 5251−5258

AUTHOR INFORMATION

Corresponding Authors

Giuseppe Mele − *Department of Engineering for Innovation, University of Salento, Lecce 73100, Italy;* orcid.org/0000-0002-6684-990X; Email: giuseppe.mele@unisalento.it

Francesca M. Toma − *Joint Center for Artificial Photosynthesis and Chemical Sciences Division, Lawrence Berkeley National Laboratory, Berkeley 94720, California, United States;* orcid.org/0000-0003-2332-0798; Email: fmtoma@lbl.gov

Authors

Alberto De Riccardis − *Department of Engineering for Innovation, University of Salento, Lecce 73100, Italy; Joint Center for Artificial Photosynthesis, Lawrence Berkeley National Laboratory, Berkeley 94720, California, United States*

Michelle Lee − *Department of Chemistry and Chemical Biology, Cornell University, Ithaca 14850, New York, United States; Chemical Sciences Division, Lawrence Berkeley National Laboratory, Berkeley 94720, California, United States;* orcid.org/0000-0002-5341-4261

Roman V. Kazantsev − *Joint Center for Artificial Photosynthesis and Chemical Sciences Division, Lawrence Berkeley National Laboratory, Berkeley 94720, California, United States*

Alejandro J. Garza − *Joint Center for Artificial Photosynthesis and Chemical Sciences Division, Lawrence Berkeley National Laboratory, Berkeley 94720, California, United States*

Guosong Zeng − *Joint Center for Artificial Photosynthesis and Chemical Sciences Division, Lawrence Berkeley National Laboratory, Berkeley 94720, California, United States*

David M. Larson − *Joint Center for Artificial Photosynthesis, Lawrence Berkeley National Laboratory, Berkeley 94720, California, United States*

Ezra L. Clark − *Joint Center for Artificial Photosynthesis and Chemical Sciences Division, Lawrence Berkeley National Laboratory, Berkeley 94720, California, United States; Department of Chemistry, University of California, Berkeley 94720, California, United States*

Peter Lobaccaro − *Joint Center for Artificial Photosynthesis, Chemical Sciences Division, and Material Science Division, Lawrence Berkeley National Laboratory, Berkeley 94720, California, United States*

Paul W. W. Burroughs − *Joint Center for Artificial Photosynthesis and Chemical Sciences Division, Lawrence Berkeley National Laboratory, Berkeley 94720, California, United States*

Ermelinda Bloise − *Department of Engineering for Innovation, University of Salento, Lecce 73100, Italy*

Joel W. Ager − *Joint Center for Artificial Photosynthesis, Chemical Sciences Division, and Material Science Division, Lawrence Berkeley National Laboratory, Berkeley 94720, California, United States;* orcid.org/0000-0001-9334-9751

Alexis T. Bell − *Joint Center for Artificial Photosynthesis and Chemical Sciences Division, Lawrence Berkeley National Laboratory, Berkeley 94720, California, United States; Department of Chemistry, University of California, Berkeley 94720, California, United States;* orcid.org/0000-0002-5738-4645

Martin Head-Gordon − *Joint Center for Artificial Photosynthesis and Chemical Sciences Division, Lawrence Berkeley National Laboratory, Berkeley 94720, California, United States; Department of Chemistry, University of California, Berkeley 94720, California, United States;* orcid.org/0000-0002-4309-6669

Complete contact information is available at: https://pubs.acs.org/10.1021/acsami.9b18924

Author Contributions

The manuscript was written through contributions of all authors. All authors have given approval to the final version of the manuscript.

Funding

This material is based on work performed at the Joint Center for Artificial Photosynthesis, a Department of Energy (DOE) Energy Innovation Hub, supported through the Office of Science of the U.S. DOE under Award No. DE-SC00004993. The computational work presented here used resources of the National Energy Research Scientific Computing Center, a DOE Office of Science User Facility supported by the Office of Science of the U.S. DOE under Contract No. DE-AC02-05CH11231.

Notes

The authors declare no competing financial interest.

ACKNOWLEDGMENTS

The authors acknowledge helpful discussion with Prof. F. D. Toste, and G. Liu is gratefully acknowledged for his support with the ICP-MS measurements.

REFERENCES

(1) Chu, S.; Majumdar, A. Opportunities and Challenges for a Sustainable Energy Future. *Nature* **2012**, *488* (7411), 294−303.

(2) Griggs, D.; Stafford-Smith, M.; Gaffney, O.; Rockström, J.; Öhman, M. C.; Shyamsundar, P.; Steffen, W.; Glaser, G.; Kanie, N.; Noble, I. Policy: Sustainable Development Goals for People and Planet. *Nature* **2013**, *495* (7441), 305−307.

(3) Aresta, M.; Dibenedetto, A. Utilisation of CO_2 as a Chemical Feedstock: Opportunities and Challenges. *Dalton Trans.* **2007**, *28*, 2975−2992.

(4) Appel, A. M.; Bercaw, J. E.; Bocarsly, A. B.; Dobbek, H.; DuBois, D. L.; Dupuis, M.; Ferry, J. G.; Fujita, E.; Hille, R.; Kenis, P. J.; et al. Frontiers, Opportunities, and Challenges in Biochemical and Chemical Catalysis of CO_2 Fixation. *Chem. Rev.* **2013**, *113* (8), 6621−6658.

(5) National Resource Council *Advancing the Science of Climate Change;* National Academies Press, 2011.

(6) Stocker, T. *Climate Change 2013: The Physical Science Basis: Working Group I Contribution to the Fifth Assessment Report of the Intergovernmental Panel on Climate Change;* Cambridge University Press, 2014.

(7) Kumar, B.; Llorente, M.; Froehlich, J.; Dang, T.; Sathrum, A.; Kubiak, C. P. Photochemical and Photoelectrochemical Reduction of CO_2. *Annu. Rev. Phys. Chem.* **2012**, *63*, 541−569.

(8) Barton, E. E.; Rampulla, D. M.; Bocarsly, A. B. Selective Solar-Driven Reduction of CO_2 to Methanol Using a Catalyzed p-GaP Based Photoelectrochemical Cell. *J. Am. Chem. Soc.* **2008**, *130* (20), 6342−6344.

(9) Hori, Y.; Kikuchi, K.; Suzuki, S. Production of CO and CH_4 in Electrochemical Reduction of CO_2 at Metal Electrodes in Aqueous Hydrogencarbonate Solution. *Chem. Lett.* **1985**, *14* (11), 1695−1698.

(10) Hori, Y.; Murata, A.; Takahashi, R.; Suzuki, S. Electroreduction of Carbon Monoxide to Methane and Ethylene at a Copper Electrode in Aqueous Solutions at Ambient Temperature and Pressure. *J. Am. Chem. Soc.* **1987**, *109* (16), 5022−5023.

(11) Hori, Y. Electrochemical CO_2 Reduction on Metal Electrodes. In *Modern Aspects of Electrochemistry;* Springer, 2008; pp 89−189.

(12) Kuhl, K. P.; Cave, E. R.; Abram, D. N.; Jaramillo, T. F. New Insights into the Electrochemical Reduction of Carbon Dioxide on Metallic Copper Surfaces. *Energy Environ. Sci.* **2012**, *5* (5), 7050−7059.

(13) White, J. L.; Baruch, M. F.; Pander, J. E., III; Hu, Y.; Fortmeyer, I. C.; Park, J. E.; Zhang, T.; Liao, K.; Gu, J.; Yan, Y.; et al. Light-driven Heterogeneous Reduction of Carbon Dioxide: Photocatalysts and Photoelectrodes. *Chem. Rev.* **2015**, *115* (23), 12888−12935.
(14) Habisreutinger, S. N.; Schmidt-Mende, L.; Stolarczyk, J. K. Photocatalytic Reduction of CO_2 on TiO_2 and Other Semiconductors. *Angew. Chem., Int. Ed.* **2013**, *52* (29), 7372−7408.
(15) Morris, A. J.; Meyer, G. J.; Fujita, E. Molecular Approaches to the Photocatalytic Reduction of Carbon Dioxide for Solar Fuels. *Acc. Chem. Res.* **2009**, *42* (12), 1983−1994.
(16) Jiang, J. *Functional Phthalocyanine Molecular Materials;* Springer, 2010; Vol. *135*.
(17) Sorokin, A. B. Phthalocyanine Metal Complexes in Catalysis. *Chem. Rev.* **2013**, *113* (10), 8152−8191.
(18) Zhang, Z.; Xiao, J.; Chen, X.-J.; Yu, S.; Yu, L.; Si, R.; Wang, Y.; Wang, S.; Meng, X.; Wang, Y.; Tian, Z.-Q.; Deng, D. Reaction Mechanisms of Well-Defined Metal−N4 Sites in Electrocatalytic CO_2 Reduction. *Angew. Chem., Int. Ed.* **2018**, *57* (50), 16339−16342.
(19) Morlanes, N.; Takanabe, K.; Rodionov, V. Simultaneous Reduction of CO_2 and Splitting of H_2O by a Single Immobilized Cobalt Phthalocyanine Electrocatalyst. *ACS Catal.* **2016**, *6* (5), 3092−3095.
(20) Corbin, N.; Zeng, J.; Williams, K.; Manthiram, K. Heterogeneous Molecular Catalysts for Electrocatalytic CO_2 Reduction. *Nano Res.* **2019**, *12* (9), 2093−2125.
(21) Manbeck, G. F.; Fujita, E. A Review of Iron and Cobalt Porphyrins, Phthalocyanines and Related Complexes for Electrochemical and Photochemical Reduction of Carbon Dioxide. *J. Porphyrins Phthalocyanines* **2015**, *19*, 45−64.
(22) Magdesieva, T.; Yamamoto, T.; Tryk, D.; Fujishima, A. Electrochemical Reduction of CO_2 with Transition Metal Phthalocyanine and Porphyrin Complexes Supported on Activated Carbon Fibers. *J. Electrochem. Soc.* **2002**, *149* (6), D89−D95.
(23) Zhu, M.; Ye, R.; Jin, K.; Lazouski, N.; Manthiram, K. Elucidating the Reactivity and Mechanism of CO_2 Electroreduction at Highly Dispersed Cobalt Phthalocyanine. *ACS Energy Lett.* **2018**, *3* (6), 1381−1386.
(24) Zhu, M.; Yang, D.-T.; Ye, R.; Zeng, J.; Corbin, N.; Manthiram, K. Inductive and Electrostatic Effects on Cobalt Porphyrins for Heterogeneous Electrocatalytic Carbon Dioxide Reduction. *Catal. Sci. Technol.* **2019**, *9* (4), 974−980.
(25) Kadish, K. M.; Smith, K. M.; Guilard, R. *The Porphyrin Handbook: Inorganic, Organometallic and Coordination Chemistry;* Elsevier, 2000; Vol. *3*.
(26) Khenkin, A. M.; Efremenko, I.; Weiner, L.; Martin, J. M.; Neumann, R. Photochemical Reduction of Carbon Dioxide Catalyzed by a Ruthenium-Substituted Polyoxometalate. *Chem. - Eur. J.* **2010**, *16* (4), 1356−1364.
(27) Kramer, W. W.; McCrory, C. C. L. Polymer Coordination Promotes Selective CO_2 Reduction by Cobalt Phthalocyanine. *Chem. Sci.* **2016**, *7* (4), 2506−2515.
(28) Liu, Y.; McCrory, C. C. L. Modulating the Mechanism of Electrocatalytic CO_2 Reduction by Cobalt Phthalocyanine through Polymer Coordination and Encapsulation. *Nat. Commun.* **2019**, *10* (1), 1683.
(29) Costentin, C.; Savéant, J.-M.; Tard, C. Catalysis of CO_2 Electrochemical Reduction by Protonated Pyridine and Similar Molecules. Useful Lessons from a Methodological Misadventure. *ACS Energy Lett.* **2018**, *3* (3), 695−703.
(30) Acar, E. T.; Tabakoglu, T. A.; Atilla, D.; Yuksel, F.; Atun, G. Synthesis, Electrochemistry and Electrocatalytic Activity of Cobalt Phthalocyanine Complexes − Effects of Substituents for Oxygen Reduction Reaction. *Polyhedron* **2018**, *152*, 114−124.
(31) Resasco, J.; Lum, Y.; Clark, E.; Zeledon, J. Z.; Bell, A. T. Effects of Anion Identity and Concentration on Electrochemical Reduction of CO_2. *ChemElectroChem* **2018**, *5* (7), 1064−1072.
(32) Grimme, S. Supramolecular Binding Thermodynamics by Dispersion-Corrected Density Functional Theory. *Chem. - Eur. J.* **2012**, *18* (32), 9955−9964.
(33) Hatsukade, T.; Kuhl, K. P.; Cave, E. R.; Abram, D. N.; Jaramillo, T. F. Insights into the Electrocatalytic Reduction of CO_2 on Metallic Silver Surfaces. *Phys. Chem. Chem. Phys.* **2014**, *16* (27), 13814−13819.
(34) Lin, S.; Diercks, C. S.; Zhang, Y.-B.; Kornienko, N.; Nichols, E. M.; Zhao, Y.; Paris, A. R.; Kim, D.; Yang, P.; Yaghi, O. M.; Chang, C. J. Covalent Organic Frameworks Comprising Cobalt Porphyrins for Catalytic CO_2 Reduction in Water. *Science* **2015**, *349* (6253), 1208−1213.
(35) Zhang, X.; Wu, Z.; Zhang, X.; Li, L.; Li, Y.; Xu, H.; Li, X.; Yu, X.; Zhang, Z.; Liang, Y.; Wang, H. Highly Selective and Active CO_2 Reduction Electrocatalysts Based on Cobalt Phthalocyanine/Carbon Nanotube Hybrid Structures. *Nat. Commun.* **2017**, *8* (1), 14675.
(36) Cheng, T.; Xiao, H.; Goddard, W. A. Reaction Mechanisms for the Electrochemical Reduction of CO_2 to CO and Formate on the Cu(100) Surface at 298 K from Quantum Mechanics Free Energy Calculations with Explicit Water. *J. Am. Chem. Soc.* **2016**, *138* (42), 13802−13805.
(37) Linstrom, P. J. *NIST Standard Reference Database Number 69;* National Institute of Standards and Technology: Gaithersburg, MD, 2005 DOI: 10.18434/T4D303.
(38) Shen, J.; Kolb, M. J.; Göttle, A. J.; Koper, M. T. M. DFT Study on the Mechanism of the Electrochemical Reduction of CO_2 Catalyzed by Cobalt Porphyrins. *J. Phys. Chem. C* **2016**, *120* (29), 15714−15721.

https://dx.doi.org/10.1021/acsami.9b18924
ACS Appl. Mater. Interfaces 2020, 12, 5251−5258

Electronic Supporting Information for

Heterogenized Pyridine-Substituted Cobalt(II) Phthalocyanine Yields Reduction of CO_2 by Tuning the Electron Affinity of the Co Center

Alberto De Riccardis[1,2], Michelle Lee[2,3,4], Roman V. Kazantsev[2,4], Alejandro J. Garza[2,4], Guosong Zeng,[2,4] David M. Larson[2], Ezra L. Clark[2,4,5], Peter Lobaccaro[2,4,6], Paul W. W. Burroughs[2,4], Ermelinda Bloise[1], Joel W. Ager[2,4,6], Alexis T. Bell[2,4,5], Martin Head-Gordon[2,4,5], Giuseppe Mele[1]*, Francesca M. Toma[2,4]*

1 Department of Engineering for Innovation, University of Salento, via Arnesano, 73100 Lecce, Italy
2 Joint Center for Artificial Photosynthesis, Lawrence Berkeley National Laboratory, 1 Cyclotron Road, Berkeley, California 94720, USA.
3 Department of Chemistry and Chemical Biology, Cornell University, Ithaca, NY 14850, USA.
4 Chemical Sciences Division, Lawrence Berkeley National Laboratory, 1 Cyclotron Road, Berkeley, California 94720, USA.
5 Department of Chemistry, University of California, Berkeley, CA 94720, USA.
6 Material Science Division, Lawrence Berkeley National Laboratory, 1 Cyclotron Road, Berkeley, California 94720, USA.

email: giuseppe.mele@unisalento.it
email: fmtoma@lbl.gov

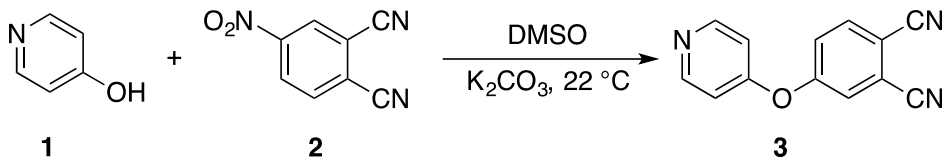

1 2 3

Scheme S1. Synthesis of 4-(4oxyPyridinyl)Phthalonitrile (**3**).

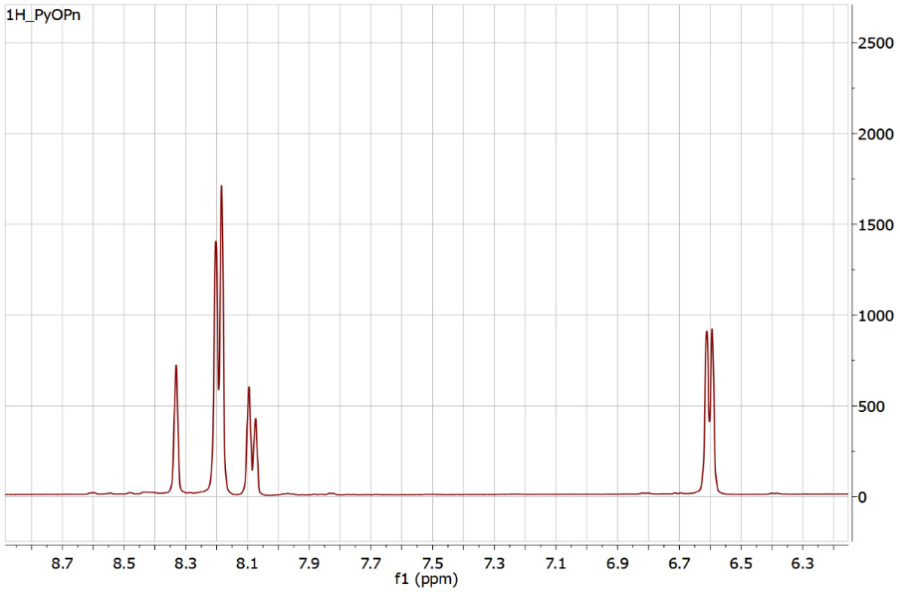

Figure S1. ^{1}H NMR (400 MHz, MeOD) of 4-(4oxyPyridinyl)Phthalonitrile (**3**): δ 8.33 (s, 1H), 8.19 (m, 3H), 8.08 (d, *J* = 8.5 Hz, 1H), 6.60 (d, *J* = 6.8 Hz, 2H).

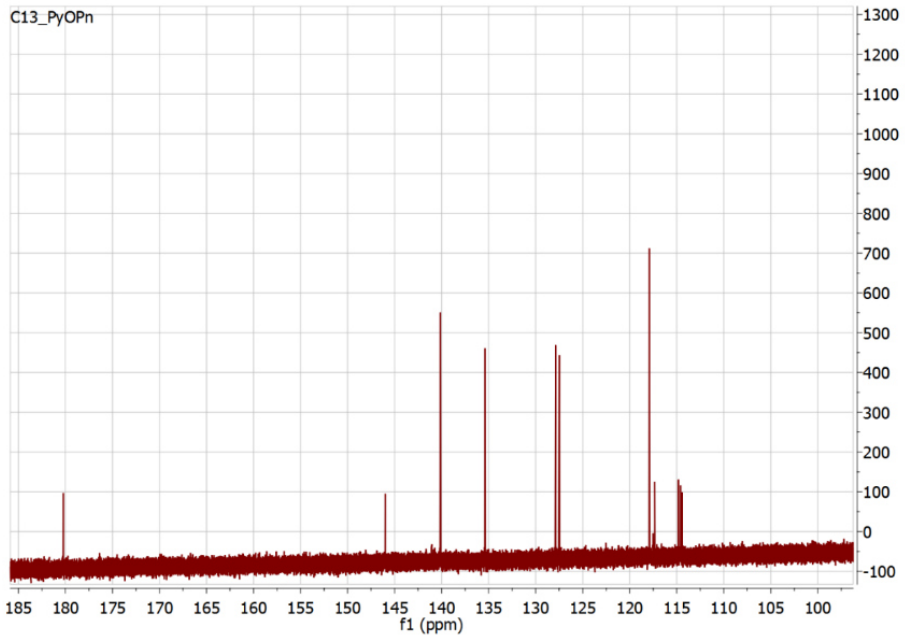

Figure S2. ^{13}C NMR (101 MHz, MeOD) of 4-(4oxyPyridinyl)Phthalonitrile (**3**): δ 180.24, 145.99, 140.12, 135.39, 127.88, 127.48, 117.91, 117.34, 114.82, 114.58, 114.41.

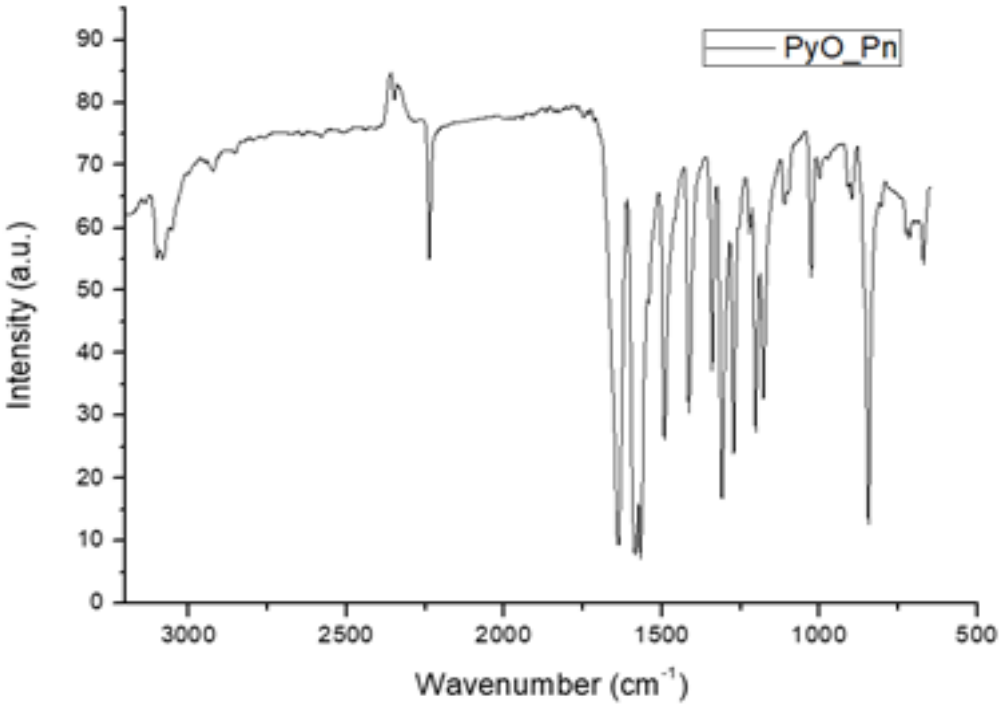

Figure S3. FTIR of 4-(4oxyPyridinyl)Phthalonitrile

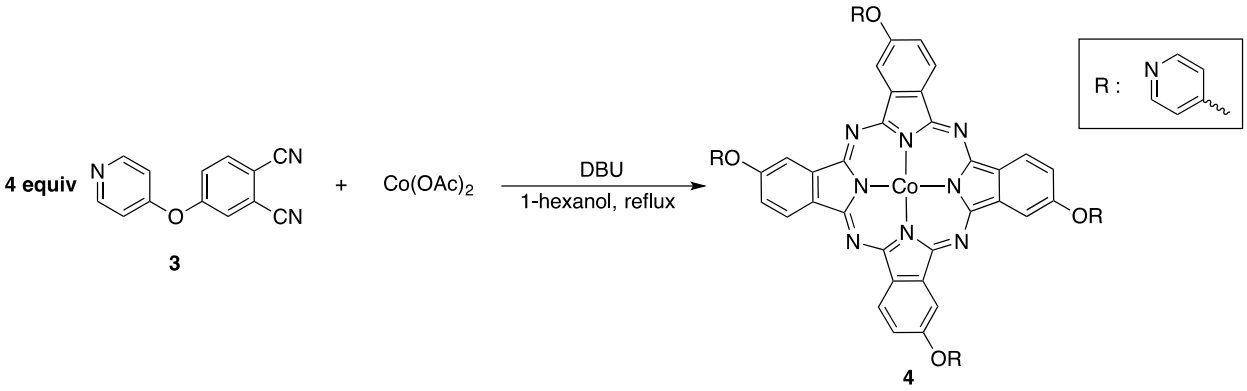

Scheme S2. Synthesis of CoPc-Pyr (**4**).

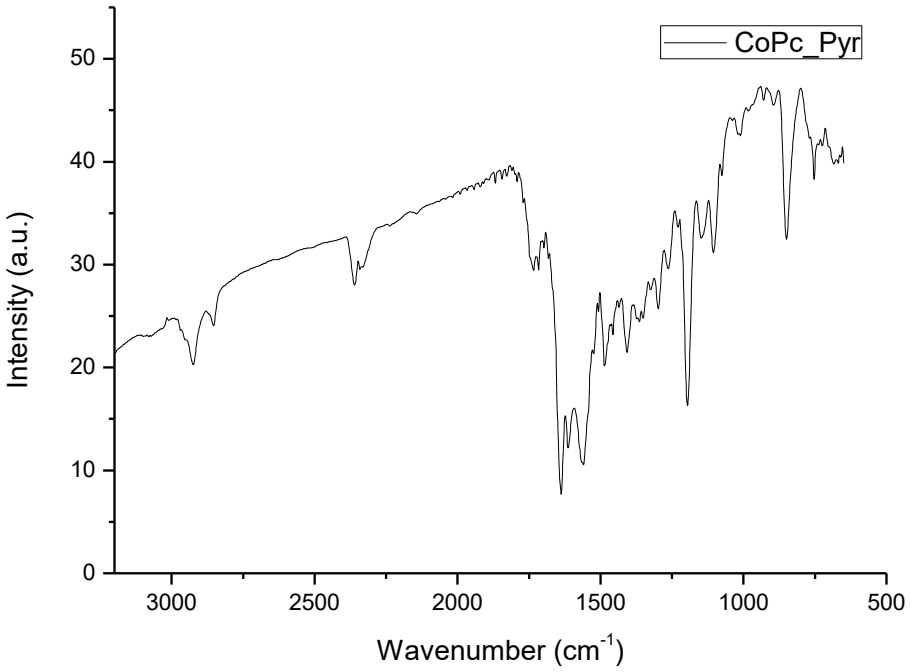

Figure S4. FTIR of CoPc-Pyr (**4**)

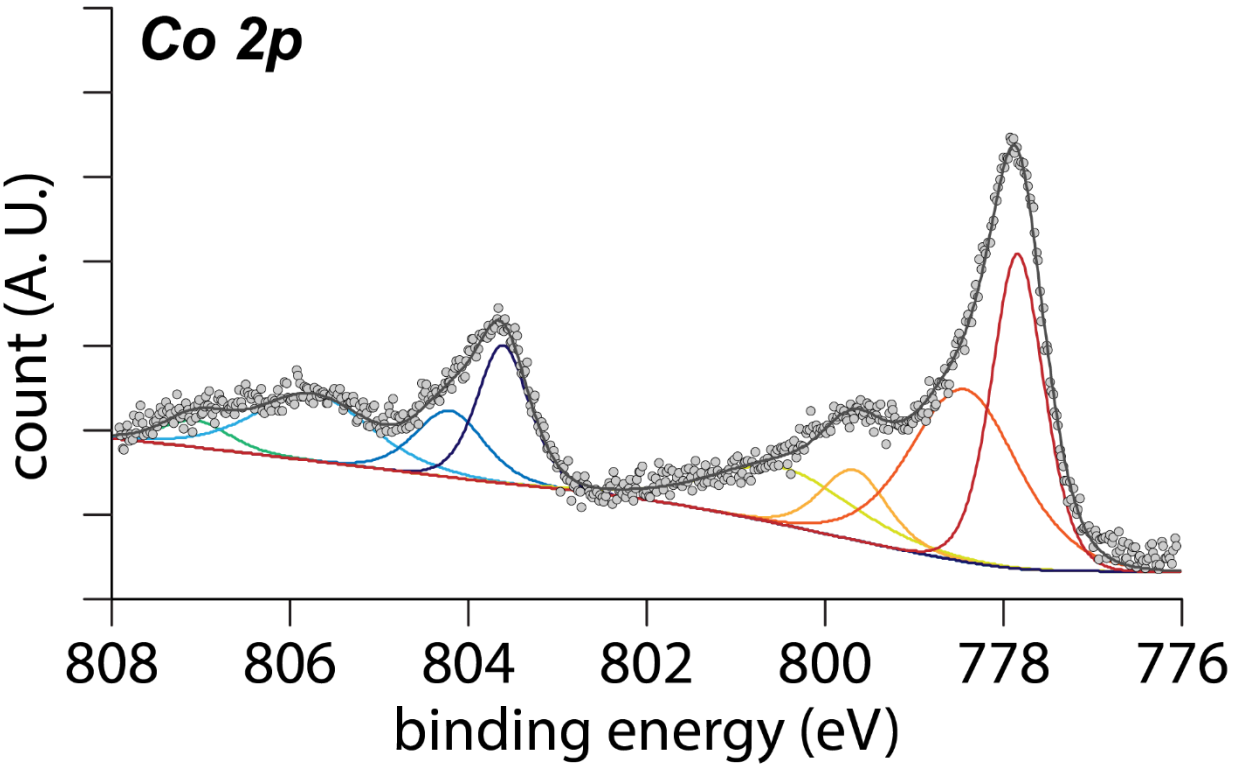

Figure S5. Co 2p XPS: Peaks at 780.9 eV, 782.5 eV, 785.8 eV, and 788 eV are assigned to the Co $2p_{3/2}$ of Co^{2+}, while the peaks at higher binding energy side are the corresponding Co $2p_{1/2}$ of Co^{2+}.[1-2]

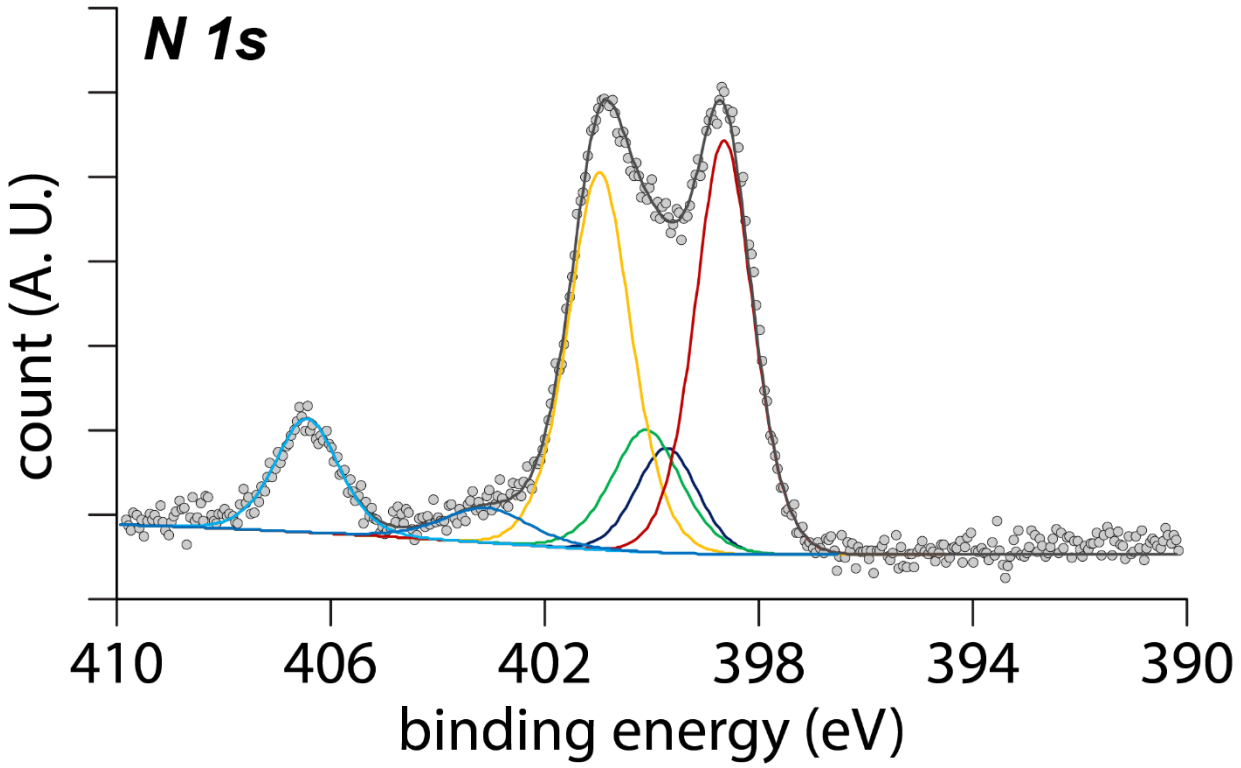

Figure S6. N 1s XPS: Peaks at 398.7 eV, 399.7 eV, 400.1 eV, 401 eV, 403.1 eV, and 406.5 eV are assigned to N – pyridyl bond, Co – N bond, N – pyrrolic bond, pyrrolic amine bond, pyridyl oxides, and NO^{2-}, respectively.[3-4]

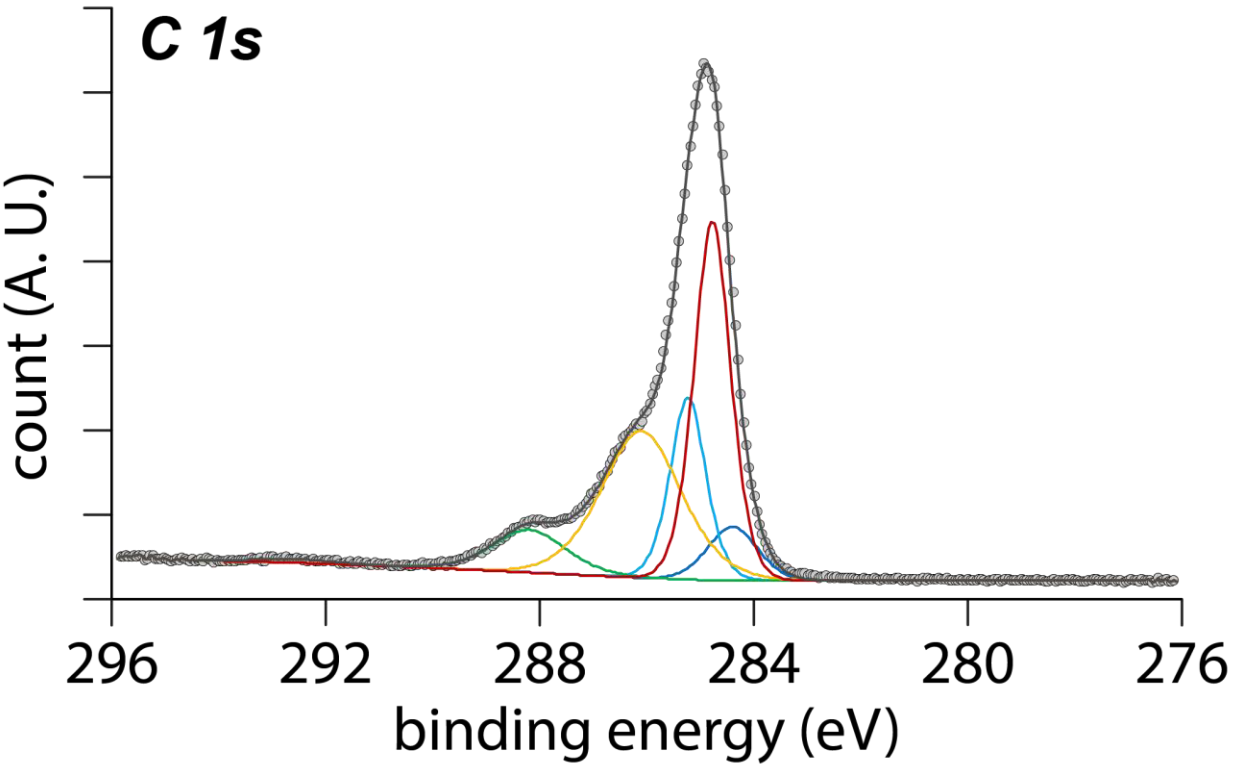

Figure S7. C 1s XPS: Peaks at 284.4 eV, 285.2 eV, 286.1 eV, and 288.2 eV are assigned to C sp2 bond, C=C bond, C – N bond, and N – C – O bond, respectively.[3-4]

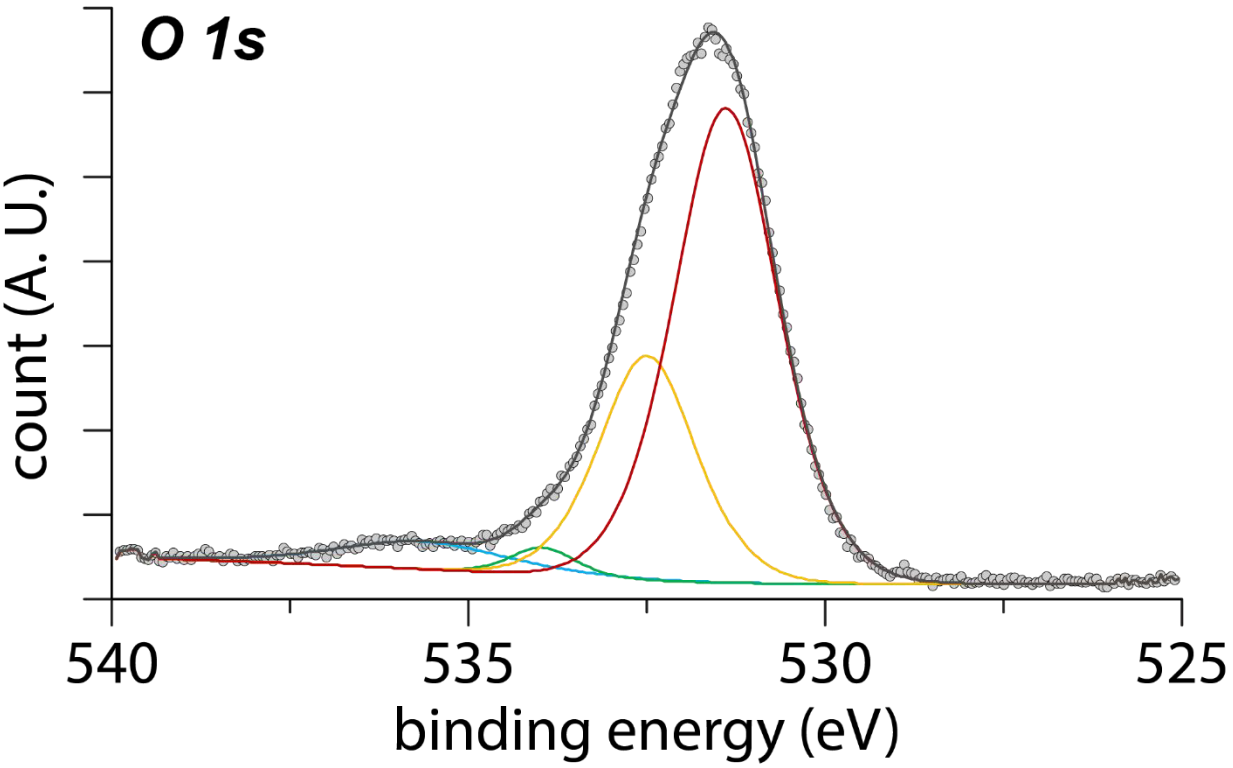

Figure S8. O 1s XPS: Peaks at 531.4 eV, 532.5 eV, 534 eV, and 535.7 eV are assigned to CoO, O – C – N bond, O_2 molecules and water molecules, respectively.[3, 5]

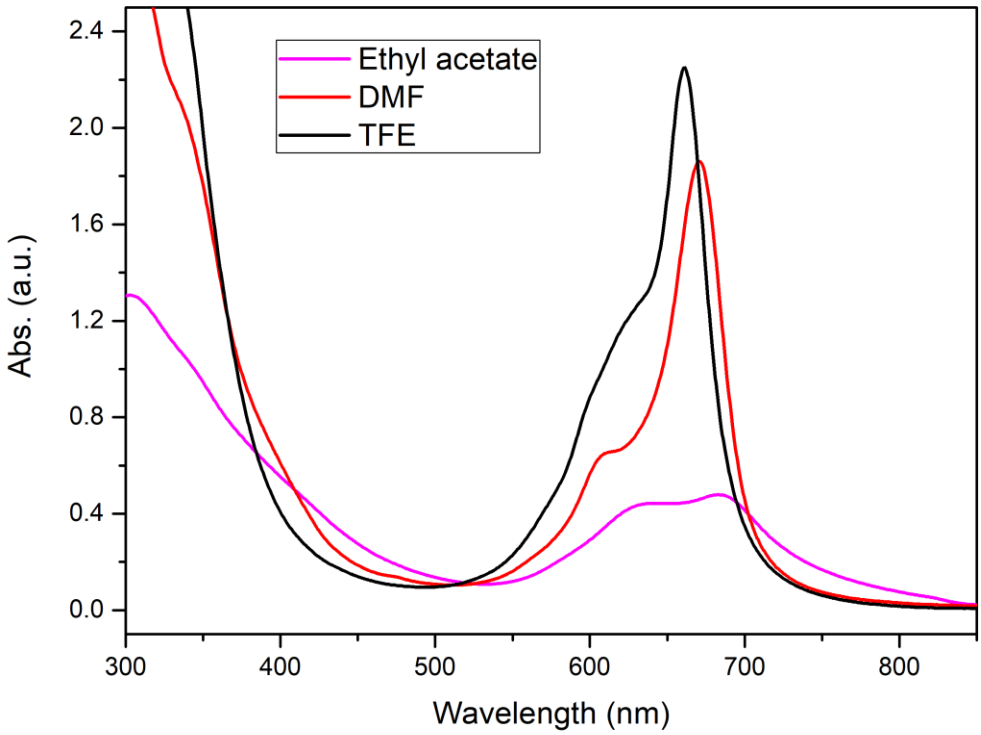

Figure S9. UV-VIS of CoPc-Pyr (**4**). The characteristic presence of the Q band[6] around 650-700 nm confirms the presence of Co in the Pc structure.

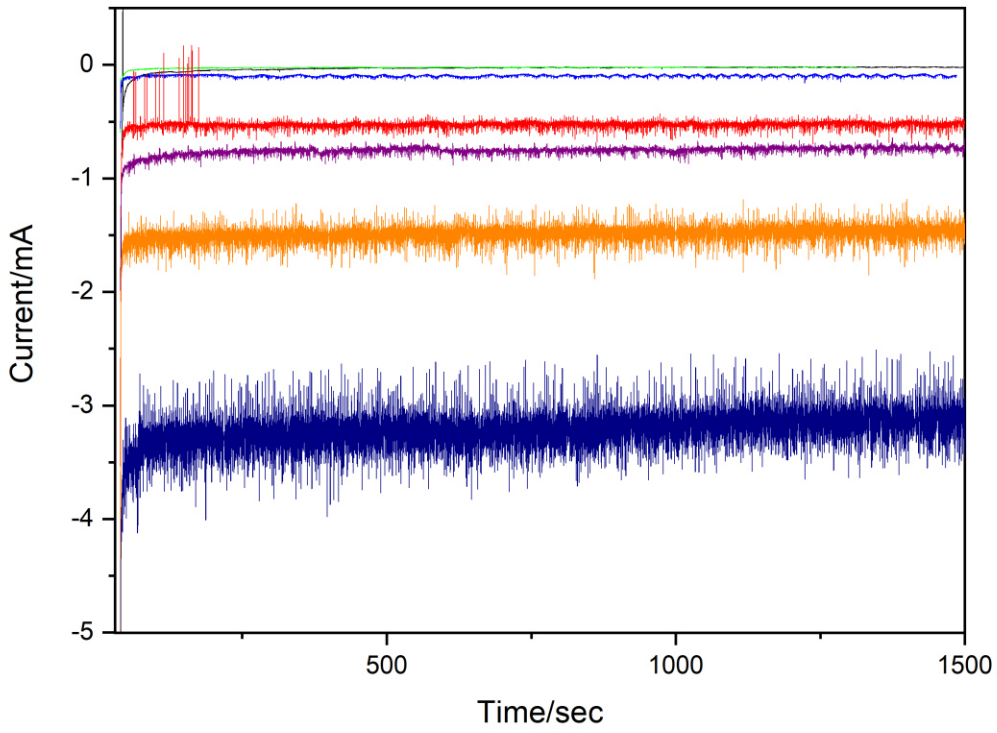

Figure S10. Chronoamperometry traces taken at 50 mV steps from -0.4 V vs RHE to -0.7 V vs. RHE. Increasing potential is correlated to increasing current, and green, black, light blue, red, purple, orange, dark blue traces correspond to -0.4, -0.45, -0.5, -0.55, -0.6, -0.65, and -0.7 V vs. RHE respectively.

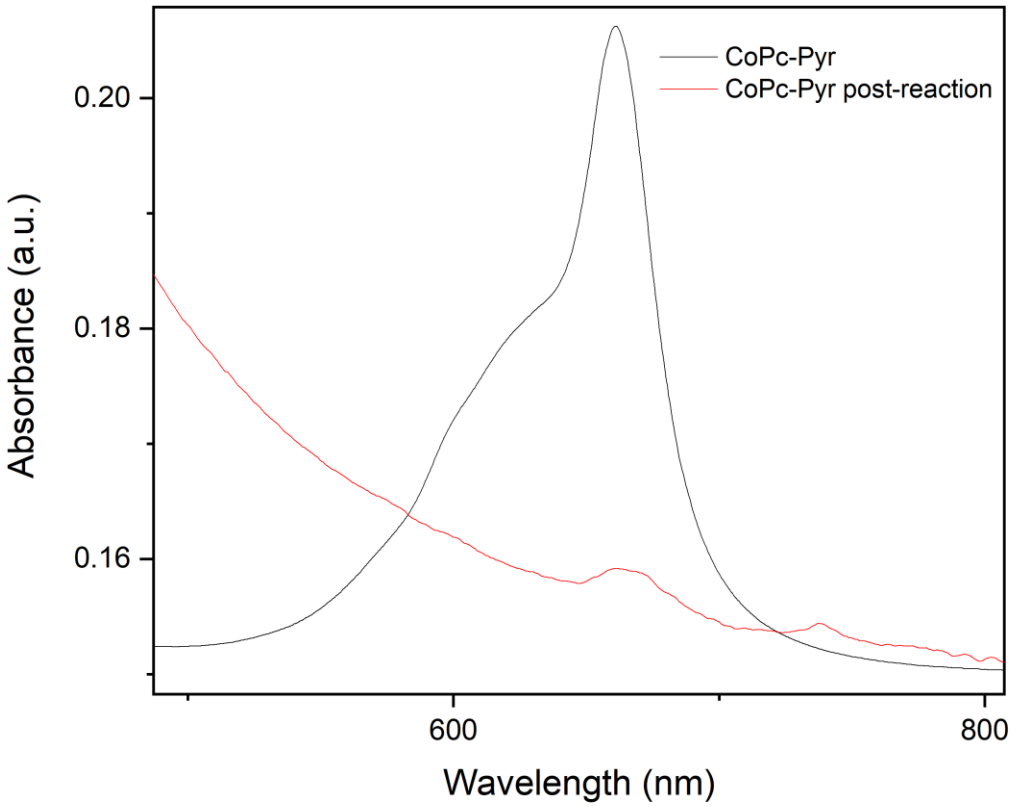

Figure S11. UV-Vis of the starting CoPc-Pyr (**4**), where acquired data has been dived by 20 times to allow for direct comparison, and of the material recovered from the electrode after the electrochemical CO_2 reduction (in black and red respectively). The characteristic Q band located at around 660 nm supports the presence of the intact Pc complex.[6] In addition, we observe the presence of an additional peak at around 740 nm. Interestingly, Q band absorption can shift with respect to the oxidation state and the counter ion of the Pc derivative, and it has been reported that Q band at longer wavelengths (as long as 760 nm) can still be observed.[6] Thus, we cannot exclude that at least some quantity of the reacted CoPc-Pyr presents a different oxidation state and counter ion that induce the Q band shift. On the other hand, metal-free Pc derivatives show Q bands at even longer wavelengths (>800 nm).[6] Thus, we can conclude that the derivative is still intact after reaction.

Table S1. Turnover frequency (TOF) calculation for CoPc-Pyr

Applied Potential (V vs RHE)	Overpotential (mV)	Current (mA)	FE for CO	TOF (s^{-1})	TOF (h^{-1})
-0.70	590	3.22	95%	6.9	24863
-0.65	540	1.74	95%	3.7	13350
-0.60	490	1.26	90%	2.5	9197
-0.55	440	0.76	80%	1.4	4946
-0.50	390	0.44	70%	0.7	2524
-0.45	340	0.19	63%	0.3	966
-0.40	290	0.06	53%	0.1	277

Table S2. Turnover frequency (TOF) calculation for CoPc

Applied Potential (V vs RHE)	Overpotential (mV)	Current (mA)	FE for CO	TOF (s^{-1})	TOF (h^{-1})
-0.80	690	4.75	96%	10	37029
-0.70	590	1.81	86%	3.5	12664
-0.60	490	0.90	79%	1.6	5741
-0.50	390	0.39	54%	0.5	1707

References

(1) Hosu, I. S.; Wang, Q.; Vasilescu, A.; Peteu, S. F.; Raditoiu, V.; Railian, S.; Zaitsev, V.; Turcheniuk, K.; Wang, Q.; Li, M.; Boukherroub, R.; Szunerits, S. Cobalt Phthalocyanine Tetracarboxylic Acid Modified Reduced Graphene Oxide: a Sensitive Matrix for the Electrocatalytic Detection of Peroxynitrite and Hydrogen Peroxide. *RSC Advances* **2015,** *5* (2), 1474-1484

(2) Biesinger, M. C.; Payne, B. P.; Grosvenor, A. P.; Lau, L. W. M.; Gerson, A. R.; Smart, R. S. C. Resolving Surface Chemical States in XPS Analysis of First Row Transition Metals, Oxides and Hydroxides: Cr, Mn, Fe, Co and Ni. *Applied Surface Science* **2011,** *257* (7), 2717-2730

(3) Artyushkova, K.; Pylypenko, S.; Olson, T. S.; Fulghum, J. E.; Atanassov, P. Predictive Modeling of Electrocatalyst Structure Based on Structure-to-Property Correlations of X-

ray Photoelectron Spectroscopic and Electrochemical Measurements. *Langmuir* **2008,** *24* (16), 9082-9088

(4) Arechederra, R. L.; Artyushkova, K.; Atanassov, P.; Minteer, S. D. Growth of Phthalocyanine Doped and Undoped Nanotubes Using Mild Synthesis Conditions for Development of Novel Oxygen Reduction Catalysts. *ACS Applied Materials & Interfaces* **2010,** *2* (11), 3295-3302

(5) Kumar, A.; Samanta, S.; Latha, S.; Debnath, A. K.; Singh, A.; Muthe, K. P.; Barshilia, H. C. Enhanced Cl_2 Sensitivity of Cobalt-Phthalocyanine Film by Utilizing a Porous Nanostructured Surface Fabricated on Glass. *RSC Advances* **2017,** *7* (7), 4135-4143

(6) Wright, J.D, Phthalocyanines. In Encyclopedia of Materials: Science and Technology, Elsevier, 2001, pp 6987-6991